



# Anisotropic Study of Ti6Al4V Alloy Formed by Selective Laser Melting

WEIDONG HUANG,<sup>1,2</sup> XIAYU CHEN,<sup>1</sup> XU HUANG,<sup>1,2,3</sup>  
HUI WANG,<sup>1,2</sup> and YITAO ZHU<sup>1</sup>

1.—Academy of Mechanical and Automotive Engineering, Fujian University of Technology, Fuzhou 350118, China. 2.—Advanced Manufacturing Productivity Promotion Center of Fujian province, Fuzhou 350118, China. 3.—e-mail: Huangxu@Fjut.Edu.Cn

Selective laser melting (SLM) is a manufacturing technology that involves melting metal powder beds. Due to the temperature gradient during the course of forming, anisotropy is further caused by oriented grain growth. However, the influence of process parameters on anisotropy has not been studied. Two types of parameter scanning strategies and rotation angle increments were selected to alter the growth tendency of grains, thus affecting anisotropy. Comparing the STRIPES scanning strategy and the CHESSE strategy, the latter can restrain anisotropy, while in the former, the anisotropy of tensile stress is influenced by the layer angle increment. The maximum tensile strength of SLM-formed parts in the formed direction deviates from an angle of 60° (1235 MPa and elongation of 5.3%), and the maximum microhardness property appears at the formed direction surface, namely, the top side surface (487 HV).

## INTRODUCTION

Selective laser melting (SLM) is a kind of metal additive manufacturing. The laser beam regionally irradiates the metal powder bed, causing rapid metal melting and solidification. SLM can immediately obtain a layer of solidification metal with a certain shape. During the SLM cycles, the layers are piled up to form a three-dimensional part.<sup>1-3</sup> Due to the character of rapid melting and solidification during SLM forming, the microstructure of SLM buildings is completely different from that of foundries.<sup>4-6</sup> The high-speed solidification process will refine the grain and significantly improve the mechanical properties.<sup>7-11</sup> However, the unidirectional heat source of SLM building and layer processing also results in obvious anisotropy,<sup>12,14</sup> and the mechanical properties perpendicular to the forming direction are greatly reduced, which restricts the exertion of mechanical properties. At the same time, unpredictable anisotropy might make topological optimization of three-dimensional structure-based homogenizing materials difficult.

In many alloys, anisotropy has been observed under SLM forming. Under conventional building path planning, the microstructure and physicochemical and mechanical properties of the forming direction (parallel to the *Z* axis) are greatly different from those perpendicular to the forming direction (parallel to the *X* or *Y* axes). For the 738LC alloy, the Young's modulus of the samples parallel to the forming direction is much lower than that perpendicular to the forming direction, while the Young's modulus of the samples in the casting state is between the two.<sup>15</sup> Similar results have been found for the Hastelloy X alloy.<sup>16</sup> Corrosion experiments on TiC/Inconel 718 metal matrix composites showed that, in different directions because of different microstructures, the surface roughness changes. The corrosion resistance showed significant differences, and the *Y-Z* planes had good corrosion resistance, but the corrosion resistance of the *X-Z* planes declined because of the uneven microstructure of corrosion resistance, while the *X-Y* planes had the worst corrosion resistance due to more irregular openings.<sup>17</sup> Some researchers have focused on the anisotropy of the wear behavior of 316L alloy samples by SLM forming. It was found that, in addition to the anisotropy produced when

the scratch is perpendicular to or parallel to the molding direction, the different angles between the scratch and the scanning direction on the same surface also show significant anisotropy.<sup>18</sup> Some researchers have attempted to eliminate columnar crystal growth by electromagnetic stirring<sup>19</sup> and ultrasonic assistance.<sup>20</sup> However, because of the limitation of the molding principle in practical applications, the anisotropy associated with eliminating restrictions on technology or cost requires an economic and reliable method to avoid or reduce the anisotropy of adverse impacts on the macroperformance.

By changing the angle increment, the state of the microstructure can be changed to some extent.<sup>21-22</sup> In the SLM forming process, in most cases columnar crystals appear along the forming direction, but due to the heat dissipation environment, the preferred orientation, and convection, columnar microstructures usually do not strictly point in the vertical direction of the Z axis.<sup>23-24</sup> This makes it possible to break the continuous growth of columnar structures by changing the angle increment. In addition, it has been reported that changing the direction of the scan line is helpful in breaking the continuous growth of tissue and reducing the anisotropy.<sup>25-27</sup> Therefore, by adjusting the angle increment and scanning strategies, this study has measured the hardness and tensile properties of the built parts in different forming directions, explored the mechanism of anisotropy, and looked for ways to prevent it in order to obtain a more homogeneous microstructure by the SLM forming process.

## EXPERIMENTAL SETUP

### Experimental Materials and Devices

In the experiment, SLM-Solutions 125HL (Germany) was used as the SLM forming equipment. Argon was used as a protective gas. The material used in the experiment was Ti6Al4V powder provided by Great CAS (China) with a calibration particle size of 20–50  $\mu\text{m}$ . The elemental composition of the powder is shown in supplementary Table S1. The experimental test equipment included a Metler ME204E Analytical Balance (Switzerland), a Hitachi TM3030Plus Benchtop Scanning Electron Microscope (SEM; Japan), an Instron Electronic Universal Testing Machine (USA), a HDNS MVA-402TS Microhardness Tester (China), and a Hirox KH1300 3D Microscopic System (USA).

### Experimental Method

Before forming, the powder was dried with a vacuum dryer at 80°C for 8 h to ensure its fluidity. The substrate was sandblasted to ensure the bonding strength between the formed parts and the substrate.

A 10 mm  $\times$  20 mm  $\times$  3 mm sheet sample was prepared and used to measure the hardness and microstructure. The hardness test was carried out at room temperature. Measurement points were taken from a position near the substrate on the test surface, one point was taken every 0.2 mm, and five measurement points were taken from each sample. The measured data were averaged. Tensile samples conforming to GB/T 228.1-2010 tensile test standards were prepared. The tensile test was carried out at room temperature, and testing was repeated 5 times for each group to take the average value.

The equipment offers two scanning strategies, namely, STRIPES and CHESS. The scanning rotation angle is the included angle of the planar projection of the substrate, including the scan line, at the same position of the adjacent two layers in the SLM forming process, as shown in supplementary Fig. S1. The sample test directions of the tensile experiment are shown in supplementary Fig. S2, which are the forming direction (BD), BD deflection direction of 30°, BD deflection direction of 60°, and BD deflection direction of 90° (referred to as BD30°, BD60° and BD90°, respectively). The test surface of the forming sample of the hardness sample is parallel to the end face of the drawing sample at various angles.

In the experiment, two scanning strategies and various angle increments, were selected to study the mechanism of anisotropy in the SLM forming process. STRIPES and CHESS were selected for the scanning strategies, and 30°, 60°, and 90° were selected as the angle increments. The level of the experimental factors is shown in Table I.

## RESULTS AND DISCUSSION

### Experimental Results

The forming sample is shown in supplementary Fig. S3. The results are shown in Table S2. The standard deviations of the experimental results are shown in Table S3. The CHESS scanning strategy can inhibit the generation of anisotropy to a certain extent, regardless of the tensile properties or microhardness. There was a significant interaction between the angle increment and the scanning strategies. The scanning rotation angle did not have a significant effect on the anisotropy under CHESS scanning, while the angle increment had a significant effect on the anisotropy of SLM forming under STRIPES scanning. In the SLM forming parts, the

**Table I. The parameters and levels for the SLM anisotropy experiment**

Parameters and levels			
Scanning strategies	Stripes	Chess	–
Angle increment (°)	30	60	90

direction of the maximum tensile strength is BD60°, and the direction of the maximum hardness is the BD direction.

### Analysis of variance (ANOVA)

To analyze the effect of factors on the anisotropy of significance, all the measured parameters are measured 5 times in this paper. In order to quantify the anisotropy, a range of performances are introduced to measure the difference between the maximum and the minimum characterization of anisotropic strength. The range data are shown in Table S4. The analysis of variance of tensile anisotropy is shown in Table S5, the analysis of variance of elongation anisotropy is shown in Table S6, and the analysis of variance of microhardness anisotropy is shown in Table S7.

According to the analysis of variance, for all performances, the  $P$  values of the scan strategies and angle increments are less than 0.001. The factors play a significant role in the data. For interaction, the  $P$  value is 0.003 in tensile anisotropy, and less than 0.001 in microhardness. The interaction in these two properties is significant. However, the  $P$  value of interaction is 0.375 in elongation, but interaction is insignificant in elongation. The ANOVA models of the performances have good degrees of fitting and high reliability.

### Analysis of the Tensile Properties

#### *Analysis of the Tensile Strength*

The tensile strength and elongation test results were visualized, as shown in Fig. 1. Comparing Fig. 1a and b, the samples of the STRIPES strategy under the same angle increments had greater differences in values of tensile strength ( $\Delta S$ ) than those of the CHESS strategy, representing obvious anisotropy. The comparison between Fig. 1a and b and Fig. 1c and d shows that the experimental groups with higher tensile strength had lower plasticity, while the group with lower tensile strength had higher elongation. Groups of BD60° showed the strongest properties.

The BD90° test surfaces of the experimental group with the most significant anisotropy (STRIPES strategy and 60° angle increment) and the least significant anisotropy (CHESS strategy and 30° angle increment) were polished to observe the microstructure, as shown in Fig. 2. Both significant groups, as shown in Fig. 2a and b, and nonsignificant groups, as shown in Fig. 2c and d, are dominated by acicular  $\alpha'$  and lamellar  $\alpha$  on the test surface of BD90° (similar to Ref. 28). However, the growth trend of acicular  $\alpha'$  was similar in the significant groups, and the acicular  $\alpha'$  phases with the same trend were connected by lamellar  $\alpha$  with a fishbone distribution (similar to Ref. 29), while there was no obvious feature in the nonsignificant group. Therefore, inner-grain fractures of acicular  $\alpha'$

and grain boundary fractures of lamellar  $\alpha$  mainly occurred when stretching along the BD direction, and grain boundary fracture of acicular  $\alpha'$  and lamellar  $\alpha$  mainly occurred when stretching along the BD90° direction. The grain boundary has a higher strength than the inner-grain, so the group shows significant anisotropy. In Fig. 2a and b, the acicular  $\alpha'$  is not strictly parallel to the forming direction but diverges by a certain angle. Therefore, the optimal tensile strength is located in the direction of BD60°, which is also observed in Ref. 30.

Observing the fracture morphology of significant groups, a large number of lamellar cleavage fracture features with a small number of dimples can be observed, as shown in Fig. 3a, indicating that the fracture in this state is mainly brittle fracture. Upon further enlarging the fracture, it can be seen that there are clear martensite grain boundaries on the lamellar cleavage characteristics, as shown in Fig. 3c. In this state, the fracture is the inter-grain fracture with grain boundary failure, and the plasticity is low while the strength is higher, which is consistent with the experimental results and the metallographic observations. This phenomenon is mainly affected by the thermal field in the SLM forming process, and the scanning strategies and angle increment have different influencing mechanisms. The scanning strategies mainly affect the temperature field of the single layer, and the angle increment mainly affects the temperature field of the adjacent forming layer. The temperature field will affect the growth of the tissue and further affect the performance.

#### *Analysis of EBSD*

The sample (STRIPES strategy, 60° scan angle increment, BD90° surface) was analyzed by electron backscatter diffraction (EBSD), as shown in Fig. 4. The neighboring grain misorientation angle distribution of the sample is shown in Fig. 4a. It can be seen that the misorientation angles of adjacent grains are shown as three peak values. The first peak is fixed on the 0° misorientation angle, called the low-angle boundary, which indicates that the partial crystals have the same or similar crystal orientation. This might be caused by a small amount of dislocation brought about by the thermal stress of rapid solidification. The second and third peaks are present at around the 60° misorientation angle (leading status, accounting for 71%) and around 90° misorientation angle (accounting for 13%). This indicates that the sample in this state has an obvious preferred orientation, which verifies that the microstructure is in a fishbone-like directional growth state as mentioned above. Grain orientation of the sample is as shown in Fig. 4b. It can be seen that different primary  $\beta$  columnar grains have different orientations, and that the same  $\beta$  grains contain martensite grains with similar orientations.<sup>31</sup> These clustered martensite grains with similar orientations result in

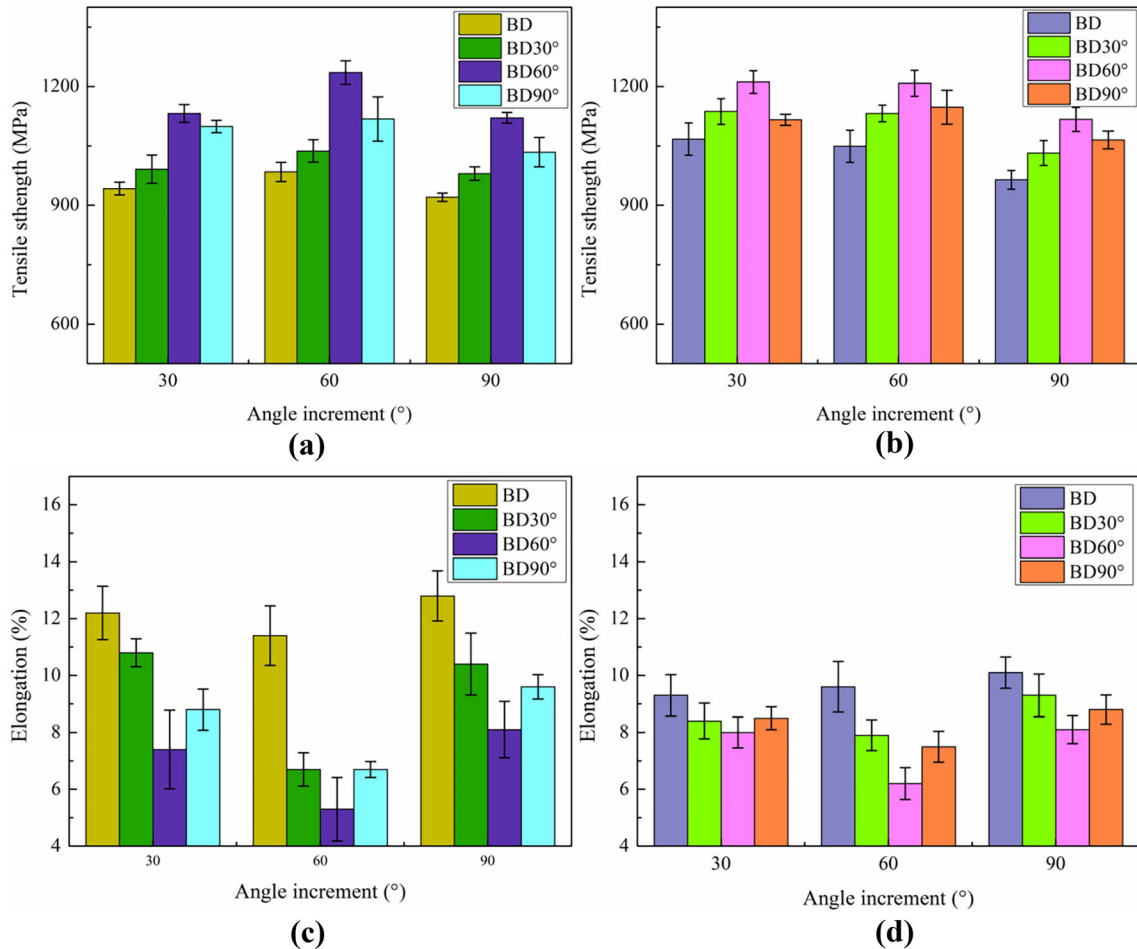


Fig. 1. Influence of the angle increment on the tensile strength and elongation in each test direction under different scanning strategies: (a) tensile strength of STRIPES strategy, (b) Tensile strength of CHES strategy, (c) elongation of STRIPES strategy, (d) elongation of CHES strategy.

macroscopic anisotropy. A sample pole diagram is shown in Fig. 4c, from which it can be seen that the preferred orientation of the sample concentrates on the  $\{0001\}$  crystal plane, and the maximum mud density is 11.25. Compared with the standard projection diagram (shown in Fig. S4), it can be seen that the grain orientations of the sample are mainly concentrated in the orientation of  $(\bar{1}\bar{1}22)$ ,  $(\bar{1}102)$  and  $(1\bar{2}12)$ .

#### Analysis of the Impact of the Parameters

Different scanning strategies will result in different laser scanning positions and sequences, which will directly affect the distribution of the temperature field.<sup>32</sup> The scanning strategy of STRIPES has continuity in monolayer scanning, and the grains tend to grow in a similar direction under continuous laser scanning.<sup>33</sup> However, the scanning lines in the adjacent scanning areas are orthogonal to each other, and the continuity of the scanning lines is poor, which is conducive to breaking the continuous growth of the grains. At the same time, under the CHES system, the scanning areas in the same

direction are scanned in succession. Therefore, when scanning in the orthogonal direction, the generated thermal field will be maintained in the scanning areas that were completed for the previous temperature to a certain extent, reducing the cooling rate of the grain and further leading to large grain growth. STRIPES is therefore more likely to produce anisotropy than CHES.

The influence of the angle increment on the SLM forming anisotropy has an obvious interaction with the scanning strategies. When the scanning mode is CHES, the angle increment has no significant effect on the anisotropy. When the scanning mode is STRIPES, the angle increment has a more significant effect on anisotropy. In the SLM forming process, due to the influence of the temperature gradient, the columnar crystals growing vertically do not grow strictly parallel to the Z axis direction.<sup>34</sup> On the one hand, under STRIPES, when the angle increment and the diverging angle of columnar crystal growth coincide, the anisotropy reaches a maximum. The anisotropy increases first and then decreases with increasing angle. On the other hand,

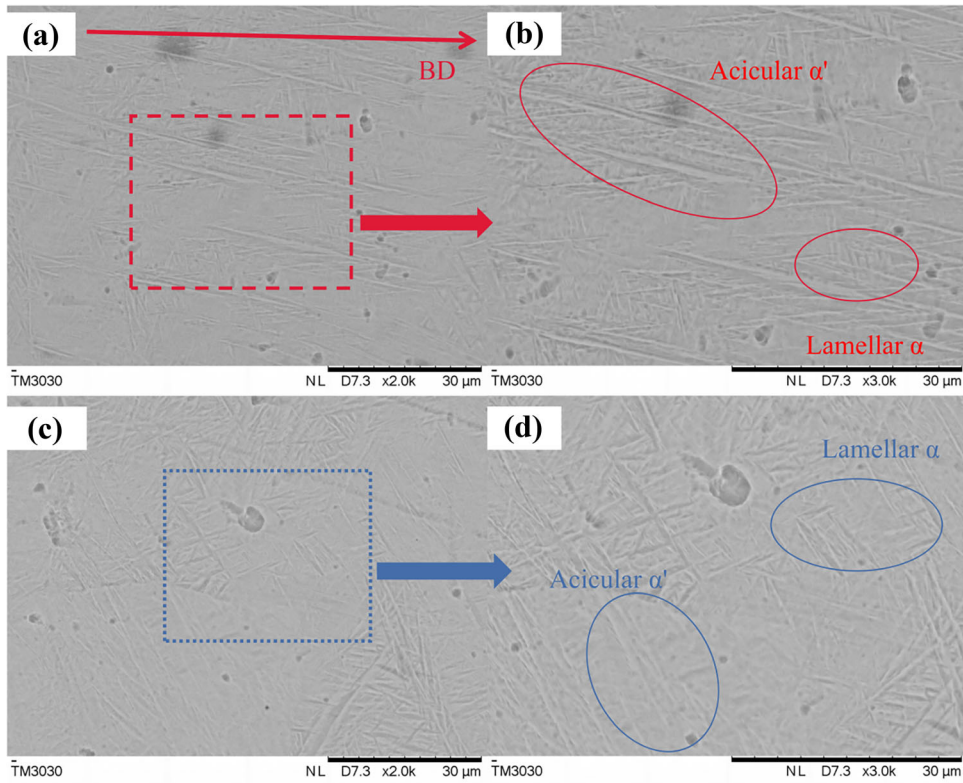


Fig. 2. Microstructure of BD90° with different scanning strategies by SEM: (a) STRIPES, ×2000, (b) STRIPES, ×3000, (c) CHES, ×2000, (d) CHES, ×3000.

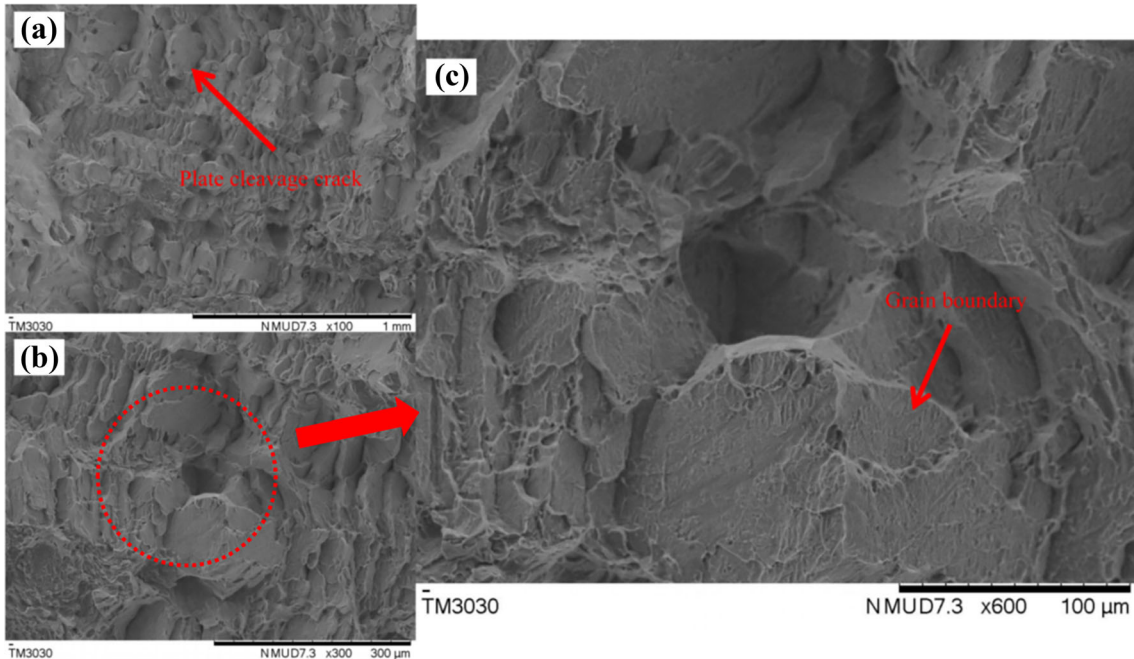


Fig. 3. Tensile fracture morphology under the STRIPES strategy by SEM, 60° angle increment and BD60° direction.

due to the diverging growth of columnar crystals, the maximum tensile strength of anisotropy due to SLM forming will occur in the direction away from the axis.

### Analysis of the Microhardness

The microhardness results are shown in Fig. 5. The maximum microhardness value is 487 HV, the minimum value is 382 HV, and the maximum

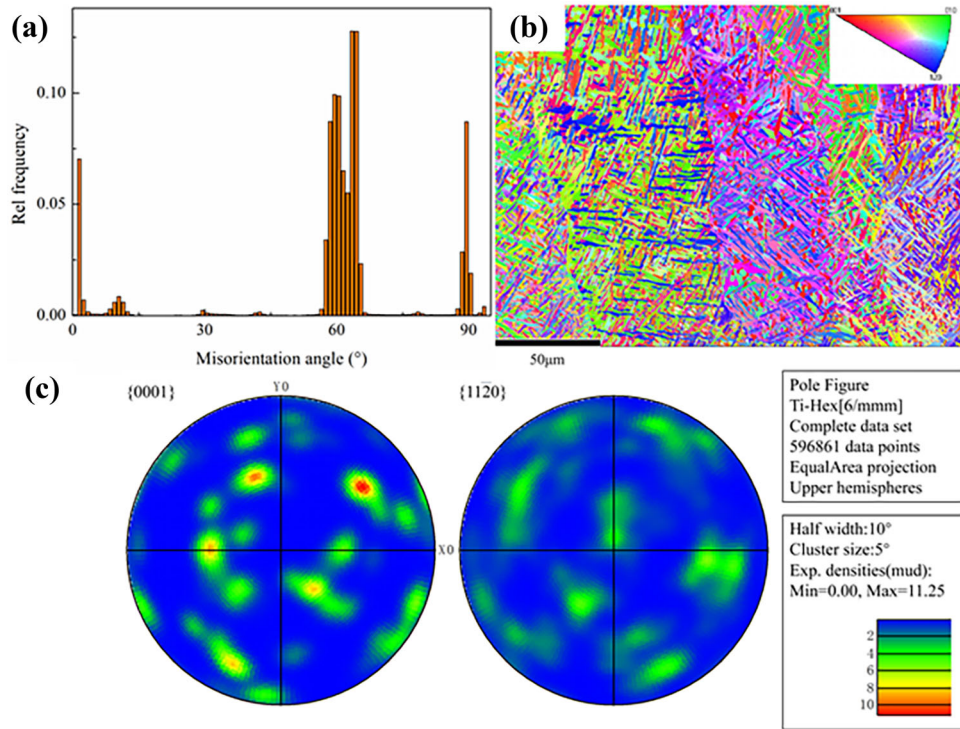


Fig. 4. EBSD analysis of SLM sample: (a) neighboring grain misorientation angle distribution (b) grain orientation, (c) pole diagram.

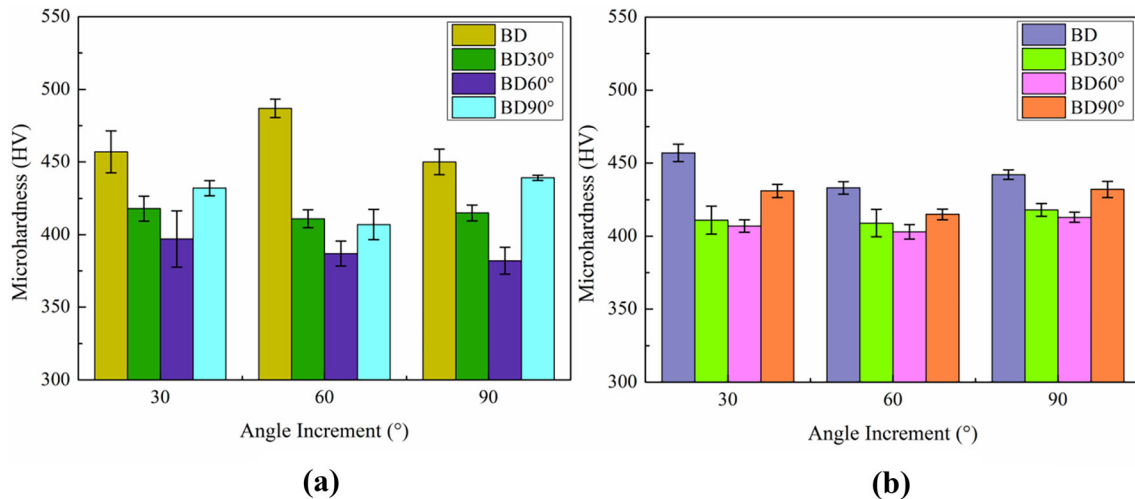


Fig. 5. Influence of the angle increment on the microhardness under different scanning strategies: (a) STRIPES strategy, (b) CHES strategy.

difference in anisotropy is 100 HV. The average hardness under STRIPES is 423.5 HV, and the average hardness under CHES is 422.5 HV. Similar to the tensile properties, the STRIPES strategy is more likely to produce anisotropy than the CHES strategy, but the expression of anisotropy is different. The maximum hardness appeared on the end face of the BD direction without deviation, and the average hardness of the samples built by CHES was significantly lower than that of STRIPES.

The characterization of microhardness is mainly reflected in the size and morphology of the grains. with the microstructures of the samples in the BD direction and the BD90° direction under STRIPES, and 60° angle increments are shown in Fig. 6a and b. The BD90° samples are mainly acicular  $\alpha'$  with large  $\beta$  columnar crystals surrounding  $\alpha'$ , while the BD samples are mainly acicular  $\alpha'$  with  $\beta$  cubic grains surrounding  $\alpha'$ . Compared with the columnar crystals, cubic grains have smaller sizes and more grain boundaries on the surface, so the BD samples show better microhardness. In addition, the

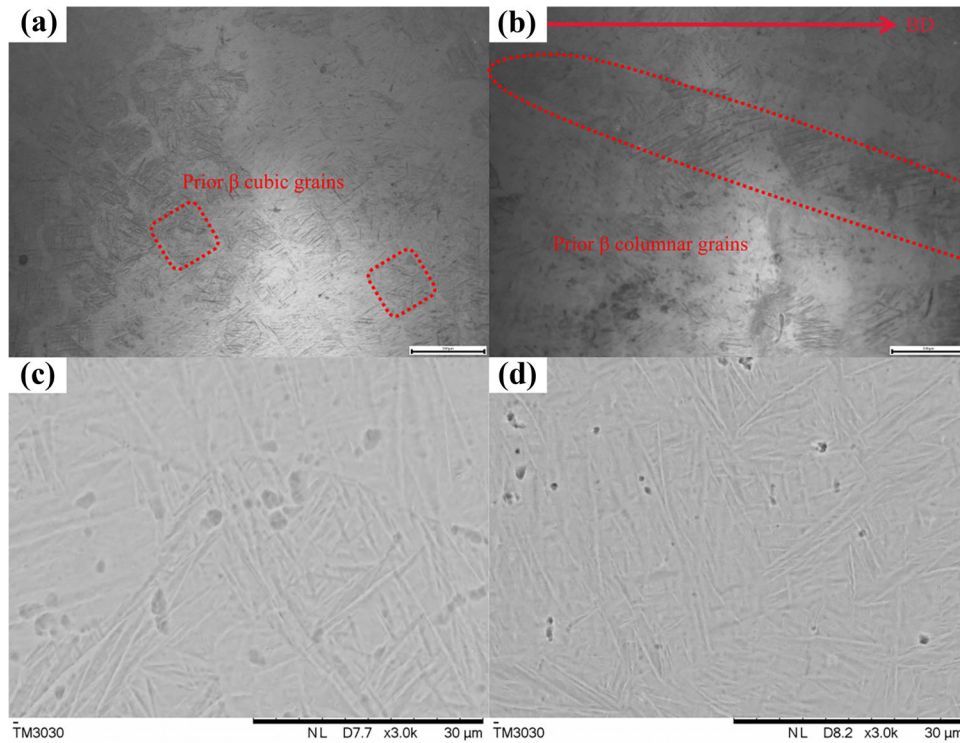


Fig. 6. Microstructure comparison for the BD direction and BD90° direction by OM: (a) BD. (b) BD90° . and grains size comparison for the CHES and STRIPES strategies by SEM. (c) CHES strategy. (d) STRIPES strategy.

microstructure of samples of the STRIPES and CHES strategies under a 60° angle increment in the BD direction are shown in Fig. 6c and d. The grain size of the CHES samples is larger, and there are fewer adjacent grain boundaries between the grains, so the hardness of the CHES samples is lower. This phenomenon is also due to the mutual insulation between adjacent grids, which reduces the temperature gradient and prolongs the growth time of the grains, so they are relatively large. From the data, the change in angle increment has limited influence on the hardness under the same scanning strategy. From the perspective of the influence mechanism, the angle increment mainly affects the bonding strength and grain growth trend between the adjacent forming layers, while the microhardness is mainly affected by the size and morphology of the grains in the test surface layer. Therefore, the influence of the angle increment on the hardness is limited.

## CONCLUSION

By adjusting the scanning strategies and angle increment in the SLM forming process, the tensile properties and hardness in the BD direction, BD30° direction, BD60° direction, and BD90° direction have been tested, and the following conclusions are drawn:

1. Compared to the CHES strategy, the STRIPES strategy is more likely to produce anisotropy.

The angle increment has an obvious interaction with the scanning strategies in the tensile experiment. Under the STRIPES strategy, the 60° angle increment will make the anisotropy more significant because of the Z direction columnar crystal deviation growth, while under the CHES strategy, the anisotropy is not significantly affected.

2. The maximum tensile strength of 1235 MPa appeared at the BD60° direction, and the phenomenon of acicular  $\alpha'$  growing out of the forming direction was observed.
3. The maximum hardness was obtained due to a large number of  $\beta$  cubic grains arranged horizontally on the BD surface, and the results for the hardness in other directions did not exhibit significant differences.

## ACKNOWLEDGEMENTS

This work was supported by the Fujian Industry-University Cooperation Project (Grant No. 2020 H6018) and Fujian Innovation Center of Additive Manufacturing (Grant No. ZCZZ20-04).

## DATA AVAILABILITY

The data that support the findings in this paper are available from the corresponding authors upon reasonable request.

### CONFLICT OF INTEREST

The authors declare that they have no known competing financial interests or personal relationships that could have appeared to influence the work reported in this paper.

### SUPPLEMENTARY INFORMATION

The online version contains supplementary material available at <https://doi.org/10.1007/s11837-021-04765-0>.

### REFERENCES

1. S. Wen, K. Chen, W. Li, Y. Zhou, Q. Wei, and Y. Shi, *Mater. Des.* 175, 107811. (2019).
2. T. Amine, C.S. Kriewall, and J.W. Newkirk, *JOM* 70, 384. (2018).
3. D. Kong, C. Dong, X. Ni, and X. Li, *Npj Mater. Degrad.* 3, 24. (2019).
4. W. Li, S. Li, J. Liu, A. Zhang, Y. Zhou, Q. Wei, C. Yan, and Y. Shi, *Mater. Sci. Eng. A* 663, 116. (2016).
5. G. Matsagopane, E.O. Olakanmi, A. Botes, and S. Kutua, *JOM* 71, 1840. (2019).
6. H. Shipley, D. McDonnell, M. Culleton, R. Coull, R. Lupoi, G. O'Donnell, and D. Trimble, *Int. J. Mach. Tools Manuf.* 128, 1. (2018).
7. B. Zhang, Y. Li, and Q. Bai, *Chin. J. Mech. Eng.* 30, 515. (2017).
8. J.R. Croteau, S. Griffiths, M.D. Rossell, C. Leinenbach, C. Kenel, V. Jansen, D.N. Seidman, D.C. Dunand, and N.Q. Vo, *Acta Mater.* 153, 35. (2018).
9. R. Ma, C. Peng, Z. Cai, R. Wang, Z. Zhou, X. Li, and X. Cao, *J. Alloys Compd.* 815, 152422. (2020).
10. H. Azizi, H. Zurob, B. Bose, S.R. Ghiaasiaan, X. Wang, S. Coulson, V. Duz, and A.B. Phillion, *Addit. Manuf.* 21, 529. (2018).
11. T. Maity, N. Chaweke, J.T. Kim, J. Eckert, and K.G. Prashanth, *Manuf. Lett.* 15, 33. (2018).
12. K.V. Yang, P. Rometsch, C.H.J. Davies, A. Huang, and X. Wu, *Mater. Des.* 154, 275. (2018).
13. Z. Chen, S. Chen, Z. Wei, L. Zhang, P. Wei, B. Lu, S. Zhang, and Y. Xiang, *PNS: MI* 28, 496. (2018).
14. J.P. Best, X. Mseder, J. Michler, and A.B. Spierings, *Adv. Eng. Mater.* 21, 1801113. (2018).
15. K. Kunze, T. Etter, J. Grasslin, and V. Shklover, *Mater. Sci. Eng. A* 620, 213. (2014).
16. T. Etter, K. Kunze, F. Geiger, and H. Meidani, *IOP Conf. Ser. Mater. Sci. Eng.* 82, 012097. (2015).
17. H. Zhang, D. Gu, L. Xi, H. Zhang, M. Xia, and C. Ma, *J. Mater. Sci. Technol.* 35, 1128. (2019).
18. Y. Yang, Y. Zhu, M.M. Khonsari, and H. Yang, *Wear* 428, 376. (2019).
19. F. Liu, H. Cheng, X. Yu, G. Yang, C. Huang, X. Lin, and J. Chen, *Optics Laser Technol.* 99, 342. (2018).
20. Y. Guo, Y. Chen, L. Kang, Y. Cao, H. Qi, and S. Yang, *Metals* 9, 1111. (2019).
21. Z. Zhang, B. Chu, L. Wang, and Z. Lu, *J. Alloys Compd.* 791, 166. (2019).
22. J.H. Robinson, I.R.T. Ashton, E. Jones, P. Fox, and C. Sutcliffe, *Rapid Prototyp. J.* 25, 289. (2019).
23. Y. Wang, C. Yu, L. Xing, K. Li, J. Chen, W. Liu, J. Ma, and Z. Shen, *J. Mater. Process. Technol.* 281, 116591. (2020).
24. Q. Liu, Y. Wang, H. Zheng, K. Tang, L. Ding, H. Li, and S. Gong, *Mater. Sci. Eng. A* 660, 24. (2016).
25. J. Han, M. Wu, Y. Ge, and J. Wu, *Int. J. Adv. Manuf. Technol.* 106, 1567. (2020).
26. S. Sun, K. Hagihara, and T. Nakano, *Mater. Des.* 140, 307. (2018).
27. L. Thijs, K. Kempen, J.P. Kruth, and J.V. Humbeeck, *Acta Mater.* 61, 1809. (2013).
28. D. Agius, K.I. Kourousis, C. Wallbrink, and T. Song, *Mater. Sci. Eng. A* 701, 85. (2017).
29. M. Wu, P. Lai, and J. Chen, *Mater. Sci. Eng. A* 650, 295. (2016).
30. W. Sun, Y. Ma, W. Huang, W. Zhang, and X. Qian, *Int. J. Fatigue* 130, 105260. (2020).
31. J. He, D. Li, W. Jiang, L. Ke, G. Qin, Y. Ye, Q. Qin, and D. Qiu, *Materials* 12, 321. <https://doi.org/10.3390/ma12020321> (2019).
32. X. Miao, X. Liu, P. Lu, J. Han, W. Duan, and M. Wu, *Metals* 10, 1379. (2020).
33. D. Wang, S. Wu, Y. Yang, W. Dou, S. Deng, Z. Wang, and S. Li, *Materials* 11, 1821. (2018).
34. J. Akram, P. Chalavadi, D. Pal, and B. Stucker, *Addit. Manuf.* 21, 255. (2018).

**Publisher's Note** Springer Nature remains neutral with regard to jurisdictional claims in published maps and institutional affiliations.